Ion Trapping and Acceleration at Dipolarization Fronts: High-Resolution MHD/Test-Particle Simulations

A. Y. Ukhorskiy[1], K. A. Sorathia [1], V. G. Merkin[1], M. I. Sitnov[1], D. G. Mitchell[1], and M. Gkioulidou[1]

[1]Johns Hopkins University, Applied Physics Laboratory, Laurel, MD USA

Key Points:

- = Energetic protons can be trapped at dipolarization fronts which enables their transport from the tail to the inner magnetosphere and violates the first invariant =
- = Trapping is important for the buildup of ion pressure in the inner magnetosphere =
- = Acceleration of trapped ions is proportional to ion charge and is independent of mass =

Abstract

Much of plasma heating and transport from the magnetotail into the inner magnetosphere occurs in the form of mesoscale discrete injections associated with sharp dipolarizations of magnetic field (dipolarization fronts). In this paper we investigate the role of magnetic trapping in acceleration and transport of the plasmasheet ions into the ring current. For this purpose we use high-resolution global MHD and three-dimensional test-particle simulations. It is shown that trapping, produced by sharp magnetic field gradients at the interface between dipolarizations and the ambient plasma, affect plasmasheet protons with energies above approximately 10 keV, enabling their transport across more than 10 Earth radii and acceleration by a factor of 10. Our estimates show that trapping is important to the buildup of the ring current plasma pressure of injected particles; depending on the plasmasheet temperature and energy spectrum, trapped protons can contribute between 20% to 60% of the plasma pressure. It is also shown that the acceleration process does not conserve the particle first invariant; on average protons are accelerated to higher energies compared to a purely adiabatic process. We also investigate how trapping and energization varies for deferent ions species and show that, in accordance with recent observations, ion acceleration is proportional to the ion charge and is independent of its mass.

1 Introduction

Energetic ($\gtrsim$ 10 keV) ions play an important role in plasma physics of Earth's inner magnetosphere. During geomagnetic storms the plasma pressure associated with strongly enhanced energetic ion populations drives a global current system that couples the inner magnetosphere and the ionosphere [e.g., *Vasyliunas*, 1984; *Roelof et al.*, 2004]. Known as the ring current, during storm enhancements it produces large distortions of magnetic field over the outer radiation belt zone, causing rapid dropouts of radiation belt intensities via adiabatic cooling and losses through the magnetopause boundary [e.g., *Kim et al.*, 2008; *Turner et al.*, 2014; *Ukhorskiy et al.*, 2015]. Energetic ions also provide the energy source for a wide range of instabilities that generate plasma waves that can resonantly accelerate high energy electrons and ions as well as cause their pitch-angle scattering and loss through precipitation into the atmosphere [see reviews, *Millan and Thorne*, 2007; *Thorne*, 2010].

The buildup of energetic ions in the inner magnetosphere is a consequence of enhanced earthward magnetospheric convection, which largely occurs in the form of mesoscale (i.e., the azimuthal scale of the order of Earth's radius) plasma flows preceded by sharp dipolarizations of magnetic field, often referred to as dipolarization fronts [e.g., *Sergeev et al.*, 1996; *Nakamura et al.*, 2002; *Runov et al.*, 2009; *Angelopoulos et al.*, 2013].

While it is well established observationally that dipolarization fronts are often associated with rapid enhancements of energetic ion intensities [e.g., *Gabrielse et al.*, 2014; *Liu et al.*, 2016], energization and transport mechanisms that produce these enhancements are a subject of ongoing debate. One common theory supported by multiple model simulations, including test-particle tracing in dipolarization fields from a magnetohydrodynamic (MHD) model [see review, *Birn et al.*, 2012] suggests that the observed enhancements are associated with ion energization obtained over a single ion interaction with the front, i.e., over the portion of the dawn-dusk ion motion traversing through the electric field pulse. On the other hand, *Zhou et al.* [2010, 2011] pointed out that since in the magnetotail the magnetic field amplitude ahead of the front can be much smaller that the field amplitude behind the front, ions can be substantially energized by reflection from a propagating fronts, similar to particle reflection from quasi-perpendicular shocks [e.g., *Terasawa*, 1979; *Gosling et al.*, 1982]. If a front is preceded with a negative magnetic field depletion, ions can be stably trapped at the reconnection line, formed ahead of the front, and accelerated by the electric field associated with the front motion [*Artemyev et al.*, 2012;

Ukhorskiy et al., 2013], similar to surfatron acceleration [e.g., *Sagdeev*, 1966; *Katsouleas and Dawson*, 1983].

Recently it was suggested that ion energization at dipolarization fronts can be greatly enhanced by trapping at the inverse magnetic field gradient which forms at the interface between azimuthally localized fronts and the background plasma [*Ukhorskiy et al.*, 2017]. Contrary to the conceptual picture of ion acceleration by an enhanced electric field pulse, which is limited to a single ion pass across its azimuthal extent, trapped ions can circle around the dipolarization front multiple times. Since the ambient magnetic field increases as the front propagates earthward, the magnetic flux through the ion guiding center orbits also grows, inducing the electric field which causes persistent ion acceleration.

Ukhorskiy et al. [2017] analysis was based on a simplified empirical model, which approximated dipolarization fronts with a soliton-like electromagnetic wave, thus neglecting any evolution of the front structure in the course of their earthward propagation as well as possible polarization effects (i.e., potential electric field). While it elucidated how trapping can enhance ion energization at dipolarization fronts, it remained unclear whether trapping would be stable under more realistic conditions of dynamically evolving fronts, and what role trapping might play in the buildup of energetic ion populations in the inner magnetosphere. In this paper we address both the plausibility and importance of ion trapping with the use of three-dimensional test-particle simulations of ion motion at dipolarization fronts in the Lyon-Fedder-Mobarry (LFM) high-resolution global MHD magnetospheric model [*Lyon et al.*, 2004]. In the following section we investigate whether trapping occurs at dynamically evolving dipolarization fronts. Section 3 describes estimates of the importance of trapping process to buildup of the ring current pressure in the inner magnetosphere. In Section 4, we assess to what extent proton transport and acceleration at dipolarization fronts is adiabatic, i.e., conserves the first adiabatic invariant. In Section 5, followed by conclusions, we investigate how ion trapping and energization depend on ion species.

2 Does Trapping Take Place?

High-resolution MHD simulation of the mesoscale flows that we used in this study is described in details by *Wiltberger et al.* [2015]. The LFM model was run using idealized solar wind conditions with fixed nominal values of the number density of 5 cm^{-3} and the earthward velocity of 400 km/s and the southward IMF of -5 nT. The simulation produced bursty mesoscale flows throughout the near-Earth plasmasheet down to geosynchronous altitudes with typical values of the earthward flow velocity of 500 km/s associated with magnetic dipolarizations of $\Delta B_z \simeq 10 - 30$ nT and the azimuthal electric field of 10 mV/m. The superposed epoch analysis of model results carried out with the use of the algorithm developed by *Ohtani et al.* [2004] for statistical analysis of the mesoscale flows observed by Geotail, showed a very good qualitative agreement between the simulated and observed dipolarization flows.

Proton transport and acceleration at the LFM dipolarization fronts was analyzed with the use of our three-dimensional test-particle Conserved Hamiltonian Integrator for Magnetospheric Particles (CHIMP) [e.g., *Sorathia et al.*, 2017]. To examine whether protons can be stably trapped at dynamic dipolarization fronts produced by high-resolution MHD simulations, we simulated proton interactions with an isolated dipolarization front that propagated from the outer boundary of our simulation domain down to $L = 5.75$. For the initial time of test-particle simulations we chose the moment when the maximum of the magnetic field dipolarization in the flow, $\max(\Delta B_z(z = 0))$, was at $L = 17$, where ΔB_z is the external component of the magnetic field, and $z = 0$ corresponds to the magnetic equator. Trapping is expected to take place inside the region, whose equatorial projection lies on closed contours of total magnetic field encircling the dipolarization [*Ukhorskiy et al.*, 2017], that we will refer to as "magnetic islands". Hence, to test for trapping, test-

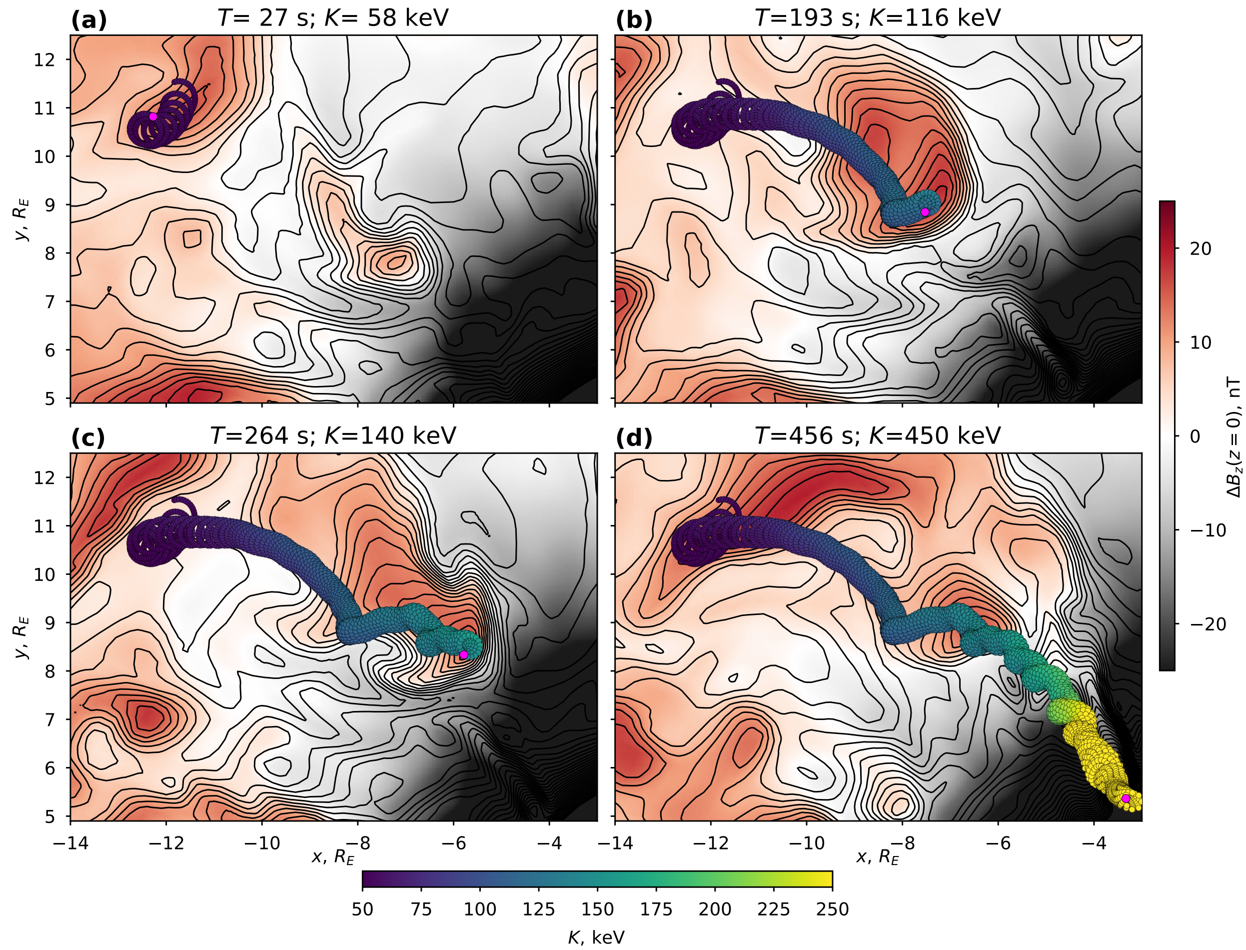

Figure 1. Proton trapping and acceleration at an isolated dipolarization front. Panels (a)-(d) show snapshots of the proton trajectory at different times of the simulation projected onto the equatorial plane; each snapshot shows the trajectory from $T = 0$ to the instance indicated by the magenta circle. Evolution of particle energy along the trajectory is indicated with color. The external magnetic field, ΔB_z, is shown with color. Contours of constant total magnetic field for each snapshots are shown with black lines.

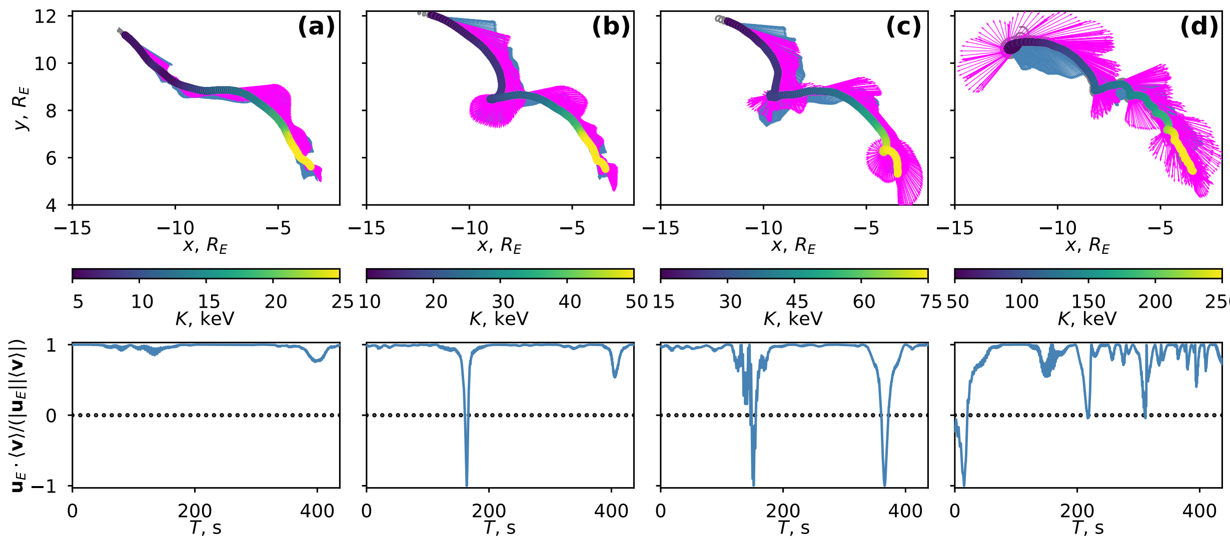

Figure 2. Proton trapping for different initial energy values. Top panels: the guiding center position estimated with a moving average is shown with symbols colored by proton energy, magenta arrows indicate current guiding-center velocity $\langle \mathbf{v} \rangle$, blue arrows show the $\mathbf{E} \times \mathbf{B}$ velocity, $\mathbf{u}_E$, at the guiding center locations. Bottom panels: the cosine between $\langle \mathbf{v} \rangle$ and $\mathbf{u}_E$; transitions from 1 to -1 values and back correspond to turning points.

particles of different initial energies were initialized at $L \simeq 17$ at the equatorial plane inside the magnetic island. To facilitate the diagnostics (see below), we suppressed test-particle bounce motion by initializing particles at near-perpendicular pitch angles.

Figure 1 and Movie S1 of the supporting information show an example of a proton trajectory for the initial energy of 50 keV; a high value of the initial energy was chosen to better illustrate the effect. Four panels in Figure 1 show snapshots of the proton trajectory at different times of the simulation; each snapshot shows the trajectory from $T = 0$ to the instance indicated by the magenta symbol. Evolution of particle energy along the trajectory is indicated with color. The proton was transported radially with the dipolarization front all the way down to the flow termination point at $L = 5.75$ being accelerated by almost a factor of 10 to 450 keV. The figure shows that by meandering about closed contours of the total magnetic field the proton remained inside the magnetic island over the entire time, i.e., was stably trapped.

Trapping is produced by the large gradients of magnetic field that are formed at the interface between dipolarization flows and the ambient plasma (see contours of total magnetic field around magnetic islands in Figure 1). If the gradient drift at the interface between a flow and the ambient plasma dominates over the $\mathbf{E} \times \mathbf{B}$ drift, protons that reach the interface are turned around by the gradient drift, which precludes them from leaving the flow. Since the effect depends on the ratio of the gradient and the $\mathbf{E} \times \mathbf{B}$ drift, it must be energy dependent.

To determine at what energies proton radial transport exhibits trapping, we used the following procedure. By applying a moving average filter to the full Lorenz proton trajectories from our test-particle simulations, we computed their guiding center position, which we then used to estimate the guiding center velocity $\langle \mathbf{v} \rangle$. The width of the moving average window for each particle was selected to roughly match its gyroperiod. We then esti-

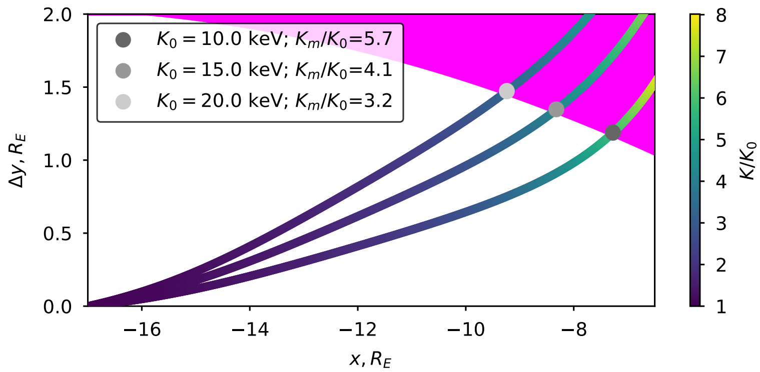

Figure 3. Equatorial proton guiding center trajectories in an azimuthally localized flow in the absence of trapping for different initial energy values; the relative change in particle initial energy is shown with color. Magenta shading indicates the flow channel boundary. Protons with initial energy $K_0 = 10$ keV and above traverse across and escape out of the flow tailward of the inner boundary at $L = 5.75$ that can be reached by trapped particles, which limits their maximum acceleration.

mated the value of the $\mathbf{E}\times\mathbf{B}$ drift $\mathbf{u}_E$ at the guiding center location and computed $\cos\alpha_{vu}$, the cosine between $\langle\mathbf{v}\rangle$ and $\mathbf{u}_E$ for each particle. Figure 2 summarizes the results for four different values of the proton initial energy: 5, 10, 15, and 50 keV. Top panels show the guiding center trajectories with symbols colored by particle energy, and $\mathbf{u}_E$ and $\langle\mathbf{v}\rangle$ vectors shown with blue and magenta. The bottom panels show $\cos\alpha_{vu}$. If $\cos\alpha_{vu} \simeq 1$ over the entire trajectory, such as in the case of a 5 keV particle shown in Figure 2(a), then the guiding center motion was governed by the $\mathbf{E}\times\mathbf{B}$ drift and trapping played no role in transporting this particle inward. If, on the other hand, at certain points of the particle trajectory $\cos\alpha_{vu}$ changed its value from 1 to -1 and then back to 1, as is the case of the particles with initial energies above 5 keV shown in Figure 2(b)-(c), the guding center velocity at these points made a full rotation around the direction of the $\mathbf{E}\times\mathbf{B}$ drift, which is the effect of trapping. The proton with initial energy of 10 keV made one full rotation (Figure 2(b)), a 15 keV proton made two rotations (Figure 2(c)). The case of a 50 keV proton (Figure 2(d)) is a bit more complicated; while from the test-particle trajectory it is apparent that the guiding center velocity rotated about the $\mathbf{E}\times\mathbf{B}$ drift multiple times, the $\cos\alpha_{vu}$ diagnostic shows only one full rotation. This is attributed to the fact that after approximately 100 s of the simulation process the proton gyroradius became comparable to the width of the dipolarization channel and to the size of the magnetic island its guiding center was rotating around. Consequently, the moving average procedure was no longer applicable for estimating the guiding center position.

According to the above analysis trapping starts affecting proton transport at the initial energies between 5 and 10 keV. It is also instructive to consider the following hypothetical question: how would particle energization change, if the mesoscale convection consisted only of the azimuthally localized intensifications of the plasma flow, i.e., there would be no magnetic islands or sharp magnetic field gradients at the interface between the flow and the ambient plasma? To answer this question, consider an equatorially mirroring guiding center particle. In the case of a purely radial flow and an azimuthally symmetric stretched magnetic configuration the guiding center motion is a superposition of the radial $\mathbf{E}\times\mathbf{B}$ drift and the azimuthal gradient drift that are related by the following equation:

$$\frac{d\varphi}{dL} = \frac{\mu c}{eR_E}\frac{1}{Lu_E(L)}\frac{d}{dL}\ln B(L) \tag{1}$$

where φ is the azimuthal angle, L is the radial distance in Earth radii denoted by R_E, μ is the first adiabatic invariant, c is the speed of light, e is the electric charge, u_E is the magnitude of the $\mathbf{E} \times \mathbf{B}$ drift, and B is the magnetic field magnitude. A proton inside a flow channel of the width Δy will undergo radial transport accompanied by adiabatic acceleration until it traverses through and escapes out of the channel due to the westward azimuthal curvature drift.

To assess the maximum acceleration that can be obtained by protons in a localized flow channel, equation (1) was integrated numerically to determine the radial distance $L_{\min}$ at which protons of different initial energy K_0 starting at the eastward edge of the flow at L_0 would reach its westward edge. The maximum energy is then given by $K_{\max} = K_0 B(L_{\min})/B(L_0)$. All parameters in equation (1) as well as the flow channel were directly inferred form the MHD and test-particle simulations. The radial dependence of $u_E(L)$ was computed at the current location of injected particles, the flow width $\Delta y(L)$ was approximated at the half maximum of $u_E(L)$, and the radial profile of $B(L)$ was estimated by fitting an exponent into the radial distribution of magnetic field along the flow channel, which was preliminary averaged over the injection time span (approximately 500 s) to remove localized dipolarizations. Figure 3 shows equatorial guiding-center trajectories of protons with initial energies of 10, 15, and 20 keV. Proton energy gain K/K_0 along the trajectories is indicated with color. As can be seen from the figure, all particles traversed across, and escaped out of the flow tailward of its earthward boundary, reached by trapped protons in test-particle simulations in self-consistent MHD fields. This simple estimate asserts that trapping is necessary for transporting 10 keV protons from the tail to the inner magnetosphere.

3 Is Trapping Important for Plasma Pressure Buildup?

In the previous section it was shown that radially transporting 10 keV protons from the tail ($L = 17$) to the inner magnetosphere ($L = 5.75$) in a single azimuthally localized ($\Delta y \lesssim 2\ R_E$) flow requires trapping. Hence, the question of whether trapping is important for building up the ring current plasma pressure is equivalent to the question of whether “seed population” protons with energies 10 keV and above at $L = 17$ provide a substantial contribution to plasma pressure in the inner magnetosphere, which is sustained by ions with energies above 10 keV [e.g., *Williams*, 1987]. It is desirable to assess the importance of trapping for various values of plasma sheet temperatures and shapes of the distribution function. For this purpose we use a Green’s function approach. We numerically derive Green’s function of a single injection in the form of a conditional probability function $W(K|K_0)$ of a proton with initial energy K_0 at $L = 17$ behind the dipolarization front to be transported to $L < 7$ with energy K. The Green’s function allows to assess how the plasmasheet proton phase space density, $f(K)$, is changed in the process of injection into the inner magnetosphere:

$$\tilde{f}(K) = \int_0^\infty W(K|K_0) f(K_0) dK_0. \tag{2}$$

We can then estimate partial contribution of the plasmasheet protons with initial energies above a certain value K_0 to the total pressure of injected particles:

$$P(> K_0) = A \int_0^\infty K^{3/2} dK \int_{K_0}^\infty W(K|K_0') f(K_0') dK_0', \tag{3}$$

where A is a normalization constant, and we assumed that the proton distribution is isotropic in pitch angle.

To derive the Green’s function we repeated test-particle simulations described in the previous section for a large ensemble of $2.5 \cdot 10^5$ particles initialized in the equatorial plane and distributed inside the magnetic island over different energy and pitch-angle values. The simulation consisted of 20 runs with initial conditions randomly distributed over the phase space variables as: 25 initial energy values between 2 and 100 keV, 5 values of the

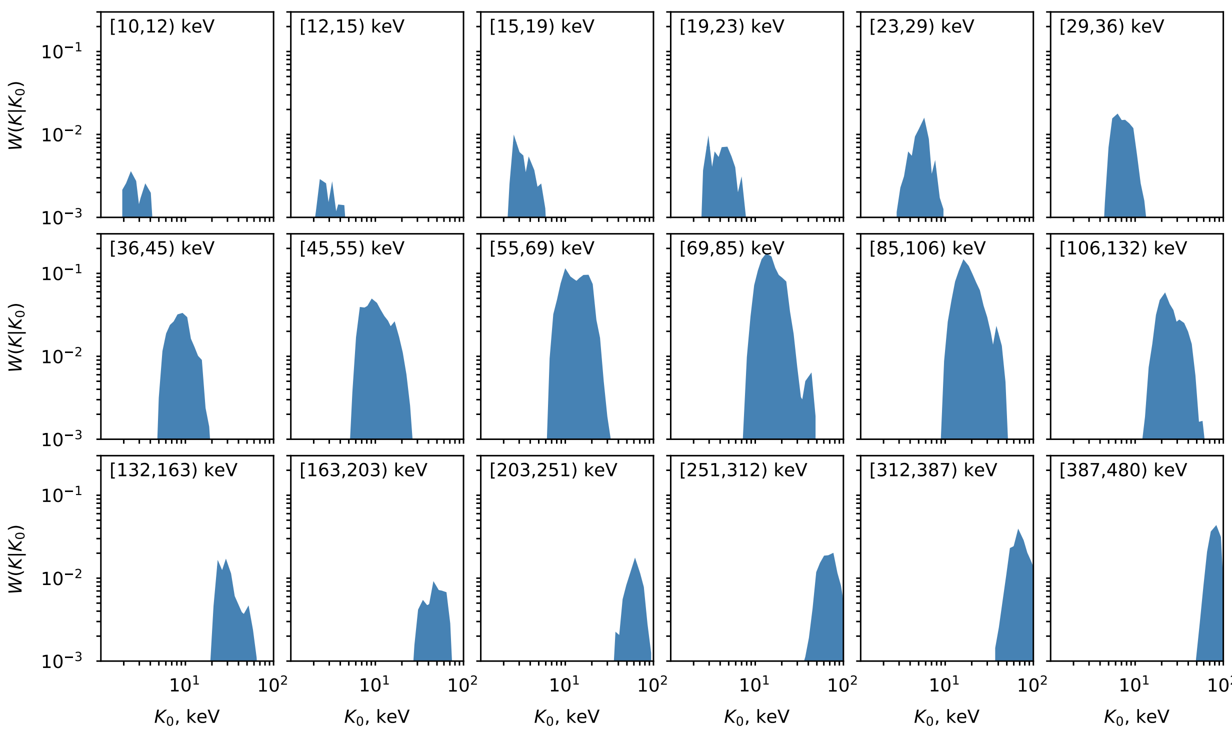

Figure 4. The Green's function $W(K|K_0)$ quantifies the probability of a proton with the initial energy K_0 at $L = 17$ behind the dipolarization front to be transported in a single injection to $L < 7$ with energy K. The figure shows $W(K|K_0)$ numerically derived from three-dimensional test-particle simulations for eighteen intervals of particle energy K at the end of the simulations.

Table 1. Partial contribution of the plasmasheet protons that exhibit trapping (i.e., have initial energy > 10 keV at $L = 17$) to the total plasma pressure of all injected particles with the initial energy of 2 keV and above, $P(K_0 > 10\,\text{keV})/P(K_0 \geq 2\,\text{keV})$, for different plasmasheet ion temperatures and κ values. The contribution varies between 20% to as much as 60%.

	$T = 1.5$ keV	$T = 3.0$ keV	$T = 5.0$ keV
$\kappa = 3$	0.35	0.51	0.61
$\kappa = 4$	0.27	0.43	0.55
$\kappa = 5$	0.22	0.38	0.60
$\kappa = 6$	0.19	0.34	0.58

pitch-angle between 10° and 90°, 10 values of L between 16.5 and 17.4, and 10 values of the azimuthal angle between 135° and 138°. The lower cut-off value of the initial energy was set to 2 keV in order to cover the full energy range of the ring current protons; in our simulations seed population protons with the initial energy of 2 keV and above at $L = 17$ constitute the bulk of greater than 10 keV protons at $L < 7$. Figure 4 shows $W(K|K_0)$ computed for different values of proton initial energy. According to the figure, the probability of being successfully transported to $L < 7$ in a single injection by an isolated dipolarization front is highest for protons with energies between approximately 35 and 100 keV. A continuous decrease in the probability values with particle energy decrease below 35 keV is attributed to the weakening of the gradient and curvature drift allowing particle escape out of the flanks of the flow channel. A decrease of the probability with the energy increase above 100 keV is associated with an increase in the proton gyroradii to the scales comparable to the size of the magnetic island, which enables their detrapping and escape out of the flow channel.

To determine the importance of trapping to the buildup of the ring current pressure, we used numerically derived $W(K|K_0)$ to compare the partial contribution of protons with the initial energy above 10 keV, which exhibit trapping, to the total plasma pressure of injected particles. For computing plasma pressure from expression (3) it was assumed that the initial phase space density of the plasma sheet ions can be approximated with a kappa distribution function. To assess the effect of trapping for different plasma sheet conditions we considered a typical range of the proton temperature and kappa exponent [e.g., *Christon et al.*, 1991]. The results are summarized in Table 1, which lists the ratios of the partial pressure of protons with the initial energy above 10 keV to the plasma pressure of all injected particles with energy of 2 keV and above, $P(K_0 > 10\,\text{keV})/P(K_0 \geq 2\,\text{keV})$. Contribution of high energy particles to the total pressure increases with increase in temperature and hardening of the spectrum, i.e., decrease in κ (as $\kappa \rightarrow \infty$ the distribution becomes Maxwellian, whereas as $\kappa \rightarrow 1$ the distribution has a power-law high energy tail). The contribution of $K_0 > 10$ keV protons to the plasma pressure of all injected particles varies from about 20% to as much as 60%. Protons transported in mesoscale localized injections account for a substantial fraction of total plasma pressure across the inner magnetosphere during storms [*Gkioulidou et al.*, 2014]. We therefore conclude that trapping is important for the buildup of the ring current pressure.

4 Is Ion Energization Adiabatic?

Observational analyses [e.g., *Runov et al.*, 2015; *Kistler et al.*, 2016] suggest that ion acceleration in the course of their inward transport from the tail into the inner magnetosphere is approximately adiabatic, i.e., conserves their first adiabatic invariant [*Alfvén*,

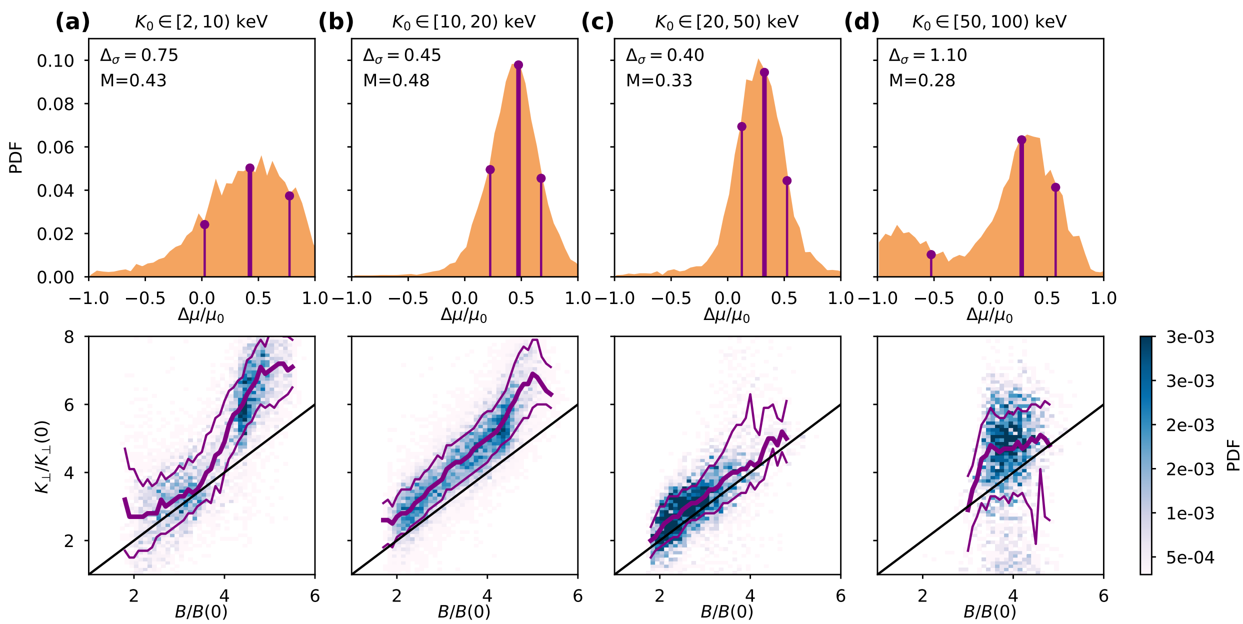

Figure 5. Proton transport and acceleration exhibit substantial deviations from purely adiabatic process at all values of proton initial energy. Top panels: distribution of the relative change in the first invariant values, $\Delta\mu/\mu_0$, at the end of the simulations; the medians (quartiles) are shown with thick (thin) magenta lines, with their numerical values indicated in the panels for each range of the initial energy. Botom panels: the dependence of ion energization on the ratio of the magnetic field amplitude at the beginning and the end of the simulations. Black lines corresponds to $K_\perp/B$ = const.

1940]:

$$\mu = \frac{(\mathbf{p}_\perp - m\mathbf{u}_E)^2}{2mB} \simeq \frac{K_\perp}{B}, \tag{4}$$

where m is the ion mass, $\mathbf{p}_\perp$ is the momentum component and $K_\perp$ is the kinetic energy perpendicular to the magnetic field at the ion gyrocenter, and B is the magnetic field amplitude. The second approximate equality is valid for nonrelativistic particles with perpendicular energy substantially exceeding the pickup energy, $mu_E^2/2$, which for the plasmasheet protons is of the order of several keV.

Test-particle simulations allow us to quantitatively assess to what degree ion transport conserves the first adiabatic invariant. For this purpose we used the ensemble simulations described in Section 2. The results are summarized in Figure 5 in two different formats. Top panels show distributions of the relative change in the invariant values, $\Delta\mu/\mu_0$, at the end of the simulations for different values of ion initial energies, whereas the bottom panels show the dependence of ion energization on the ratio of the magnetic field amplitude at the beginning and the end of the simulations. The higher is the ratio of the magnetic field amplitude at the beginning and the end of a particle trajectory, the larger is the radial distance spanned by the particle.

Figure 5 clearly shows that proton transport exhibits substantial deviations from the adiabaticity at all values of the initial energies. The difference between the upper and the lower quartiles of the $\Delta\mu/\mu_0$ distribution varies between 0.4 and 1.1. The energization process also exhibits systematic deviations from purely adiabatic acceleration. While similarly to adiabatic acceleration the proton energy increases with the increase in magnetic field experienced by the particles (equation (4)), the acceleration is higher than what would be expected in a purely adiabatic process, at all values of initial energy and regardless of the radial distance spanned by the particles (see bottom panels). The median of the $\Delta\mu/\mu_0$ distribution shifted up by 0.3-0.5, depending on the initial energy.

5 How Does Acceleration Depend on Ion Species?

Recent analysis of H, He, and O ion measurements by the RBSPICE experiment of the Van Allen Probes mission showed that the peak energy of ions injected into the inner magnetosphere is proportional to the ion charge and is independent of the mass [*Mitchell et al.*, 2018; *Motoba et al.*, 2018]. This suggests that the ratio of ion energy to the electric charge, K/q, can act as a similarity parameter of ion dynamics at dipolarization fronts. To assess whether this is the case in our test-particle simulations of trapped ions, we repeated the simulations of H^+ ions described in Sections 3 and 4 for He^+, He^{2+}, O^+, and O^{6+} ions. To compare the results with dispersed ion injections observed by RBSPICE, we introduced virtual detectors at several points of the equatorial plane. The detectors recorded the energy of test-particles when their projections onto the equatorial plane were crossing the magnetic local time meridian of the detectors within 0.25 R_E of their radial locations.

The results are summarized in Figure 6. Top panels show the locations of four virtual detectors overlaid onto equatorial projections of H^+ ions with the energy indicated with color. The equatorial projections are shown at four instances of test-particle simulation, to illustrate ion drift relative to the detector locations. The center of the dipolarization flow channel is indicated with the radial line, while the inner boundary of ion injections at $L = 5.75$ is marked with a circle. The middle panels show the energy of different ion species recorded at four detector locations as a function of time, while the bottom panel shows the ratio of ion energy to the charge state. According to the figure the injection dispersion increases as the detector location moves away from the center of the dipolarization flow, while the injection energy signature narrows down and simplifies as the detector location approaches the earthward penetration boundary. The most remarkable effect, however, which is seen at all detector locations, is the scaling in the injection signatures of all ion species by the parameter K/q.

The scaling of ion dynamics by K/q can be found somewhat counterintuitive. Indeed, the K/q similarity is an inherent attribute of the guiding center motion, for which a bounce-averaged equation can be written as:

$$\frac{d\mathbf{R}}{dt} = \mathbf{u}_E(\mathbf{R}, t) + \frac{K}{q}\mathbf{u}_D(\mathbf{R}, t), \tag{5}$$

where $\mathbf{R}$ is the guiding center position, $\mathbf{u}_E$ is the ExB drift, and $\mathbf{u}_D$ is the gradient-curvature drift. Hence, two guiding center particles with the same initial conditions and K/q ratio would exhibit the same dynamics. According to our analysis, however, ion energization at dipolarization fronts exhibits large deviations from the adiabaticity even in the case of protons. While we defer detailed investigation of this seeming contradiction to the future studies, we can speculate that it could be explained by large separation of spatial and temporal scales and consequent decoupling of non-local ion energization, due to inward radial transport, and localized invariant violation, due to pitch-angle scattering at large magnetic field curvature.

6 Conclusions

We investigated the role of magnetic trapping in transport and acceleration of energetic ions at dipolarization fronts with the use of high-resolution global MHD [*Wiltberger et al.*, 2015] and test-particle simulations. Protons were initialized inside an isolated dipolarization front at approximately $L = 17$, with energies between 2 and 100 keV, and pitch-angle values between 10° and 90°. A large fraction of protons remained trapped and propagated with the front down to $L \simeq 6$ acquiring up to a factor of 10 acceleration. The analysis of the simulation results showed that:

1. Plasmasheet protons with energies above 5-10 keV exhibit magnetic trapping. In the absence of trapping, particles would traverse across, and escape out of the front at higher L (then observed in the simulations) and consequently would not achieve full energization.
2. Trapping is important for the buildup of ion pressure in the inner magnetosphere; depending on the assumptions on the plasmasheet particle energy spectrum, trapped particles can contribute between 20% and 60% of the plasma pressure of all injected particles.
3. Proton transport and energization exhibit significant deviations from purely adiabatic acceleration. The first invariant violation, as measured by the difference between the upper and the lower quartiles of the $\Delta\mu/\mu_0$ distribution at the end of the simulation, varied between 0.4 and as much as 1.1 depending on the initial energy. Simulations also showed that, on average, the energization process is 30% to 50% more efficient than purely adiabatic acceleration.
4. A comparative analysis of different ion species, showed that our test-particle model well reproduces recent observational results, which established that acceleration of injected ions is proportional to the ion charge is independent of their mass.

Acknowledgments

= The research was supported by NSF grant AGS-1404322, NASA grant NNX16AG73G, and NASA contract NAS5-01072 through a subcontract from NJIT999640-I. We would like to acknowledge the use of computational resources (doi:10.5065/D6RX99HX) at the NCAR-Wyoming Supercomputing Center provided by the National Science Foundation and the State of Wyoming, and supported by NCAR's Computational and Information Systems Laboratory. Simulation results are available via: 10.5281/zenodo.1249722.=

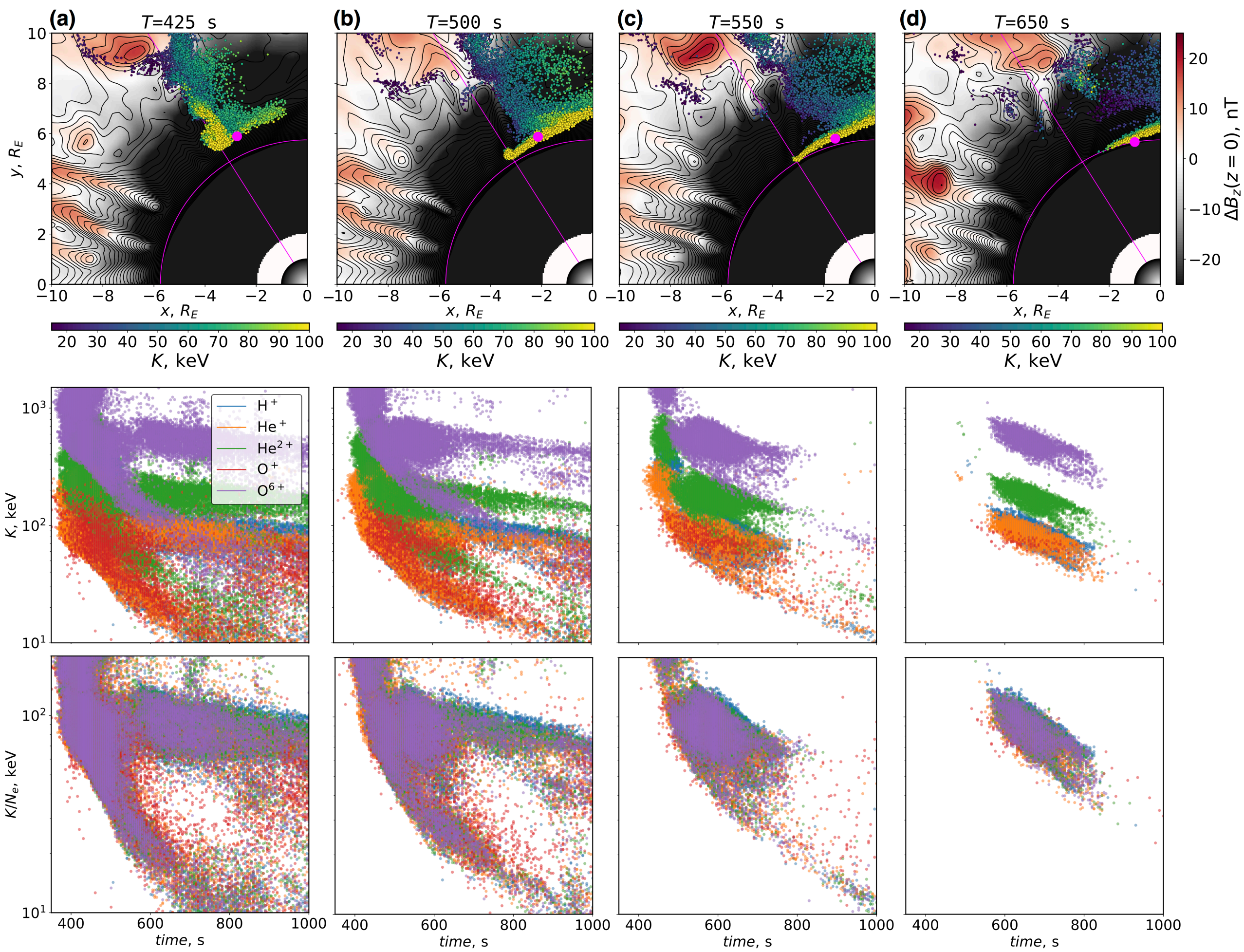

Figure 6. Ion transport and energization at dipolarization fronts scale with K/q. The figure shows inner magnetospheric injections of different ion species observed at four different locations of the equatorial plane. Top panels: detector locations overlaid onto the equatorial projection of a proton injection at different instances of the test-particle simulation; proton energy is indicated with color. The center of the injection channel is indicated with a radial line, while the inward injection boundary is marked with a circle. Middle (bottom) panels: ion energy (energy divided by the charge state) of different ion species observed at four locations.

References

Alfvén, H. (1940), On the motion of a charged particle in a magnetic field, *Ark. Mat. Astron. Fys.*, *25B(29)*, 1.

Angelopoulos, V., A. Runov, X.-Z. Zhou, D. L. Turner, S. A. Kiehas, S. S. Li, and I. Shinohara (2013), Electromagnetic energy conversion at reconnection fronts, *Science*, *341*(6153), 1478, doi:10.1126/science.1236992.

Artemyev, A. V., V. N. Lutsenko, and A. A. Petrukovich (2012), Ion resonance acceleration by dipolarization fronts: analytic theory and spacecraft observation, *Ann. Geophys.*, *30*, 316, doi:10.5194/angeo-30-317-2012.

Birn, J., A. Artemyev, D. Baker, M. Echim, M. Hoshino, and L. Zelenyi (2012), Particle acceleration in the magnetotail and aurora, *Space Sci. Rev.*, *173*, 49, doi: 10.1007/s11214-012-9874-4.

Christon, S. P., D. J. Williams, D. G. Mitchell, C. Y. Huang, and L. A. Frank (1991), Spectral characteristics of plasma sheet ion and electron populations during disturbed geomagnetic conditions, *J. Geophys. Res.*, *96*, 1.

Gabrielse, C., V. Angelopoulos, A. Runov, and D. L. Turner (2014), Statistical characteristics of particle injections throughout the equatorial magnetotail, *J. Geophys. Res.*, *119*, 2512, doi:10.1002/2013JA019638.

Gkioulidou, M., A. Y. Ukhorskiy, D. G. Mitchell, T. Sotirelis, B. H. Mauk, and L. J. Lanzerotti (2014), The role of small-scale ion injections in the buildup of EarthâĂŹs ring current pressure: Van Allen Probes observations of the 17 March 2013 storm, *J. Geophys. Res.*, *119*, 7327, doi:10.1002/2014JA020096.

Gosling, J. T., M. F. Thomsen, S. J. Bame, W. C. Feldman, G. Paschmann, and N. Sckopke (1982), Evidence for specularly reflected ions upstream from the quasi-parallel bow shock, *Geophys. Res. Lett.*, *9*, 1333.

Katsouleas, T., and J. Dawson (1983), Unlimited electron acceleration in laser-driven plasma waves, *Phys. Rev. Lett.*, *51*, 392.

Kim, K. C., D.-Y. Lee, H.-J. Kim, L. R. Lyons, E. S. Lee, M. K. Öztürk, and C. R. Choi (2008), Numerical calculations of relativistic electron drift loss effect, *J. Geophys. Res.*, *113*, A09,212, doi:10.1029/2007JA013,011.

Kistler, L. M., C. G. Mouikis, H. E. Spence, A. M. Menz, R. M. Skoug, H. O. Funsten, B. A. Larsen, D. G. Mitchell, M. Gkioulidou, J. R. Wygant, and L. J. Lanzerotti (2016), The source of o^+ in the storm time ring current, *J. Geophys. Res.*, *121*, 5333, doi:10.1002/2015JA022204.

Liu, J., V. Angelopoulos, X.-J. Zhang, D. L. Turner, C. Gabrielse, A. Runov, J. Li, H. O. Funsten, and H. E. Spence (2016), Dipolarizing flux bundles in the cis-geosynchronous magnetosphere: Relationship between electric fields and energetic particle injections, *J. Geophys. Res.*, *121*, doi:10.1002/2015JA021691.

Lyon, J. G., J. A. Fedder, and C. M. Mobarry (2004), The Lyon-Fedder-Mobarry (LFM) global MHD magnetospheric simulation code, *J. Atmos. Solar-Terr. Phys.*, *25*, 3039.

Millan, R. M., and R. M. Thorne (2007), Review of radiation belt relativistic electron losses, *J. Atmos. Solar-Terr. Phys.*, *69*, 362.

Mitchell, D., M. Gkioulidou, and A. Y. Ukhorskiy (2018), Energetic ion injections inside geosynchronous orbit: Convection and drift dominated, charge-dependent adiabatic energization (W = qEd), *J. Geophys. Res.*, *submitted*.

Motoba, T., S. Ohtani, M. Gkioulidou, A. Ukhorskiy, D. G. Mitchell, K. Takahashi, L. J. Lanzerotti, C. A. Kletzing, H. Spence, and J. R. Wygant (2018), Response of different ion species to local magnetic dipolarization inside geosynchronous orbit, *J. Geophys. Res.*, *submitted*.

Nakamura, R., W. Baumjohann, B. Klecker, Y. Bogdanova, A. Balogh, H. Réme, J. M. Bosqued, I. Dandouras, J. A. Sauvaud, K.-H. Glassmeier, L. Kistler, C. Mouikis, T. L. Zhang, H. Eichelberger, and A. Runov (2002), Motion of the dipolarization front during a flow burst event observed by Cluster, *Geophys. Res. Lett.*, *29*, 1942, doi:

doi:10.1029/2002GL015763.

Ohtani, S., M. A. Shay, and T. Mukai (2004), Temporal structure of the fast convective flow in the plasma sheet: Comparison between observations and two-fluid simulations, *J. Geophys. Res.*, *109*, A03,210, doi:doi:10.1029/2003JA010002.

Roelof, E. C., P. C. Brandt, and D. G. Mitchell (2004), Derivation of currents and diamagnetic effects from global plasma pressure distributions obtained by IMAGE/HENA, *Adv. Space. Res.*, *33*, 747.

Runov, A., V. Angelopoulos, M. I. Sitnov, V. A. Sergeev, J. Bonnell, J. P. McFadden, D. Larson, K. H. Glassmeier, and U. Auster (2009), THEMIS observations of an earthward-propagating dipolarization front, *Geophys. Res. Lett.*, *36*, L14,106, doi: doi:10.1029/2009GL038980.

Runov, A., V. Angelopoulos, C. Gabrielse, J. Liu, D. L. Turner, and X.-Z. Zhou (2015), Average thermodynamic and spectral properties of plasma in and around dipolarizing flux bundles, *J. Geophys. Res.*, *120*, 4369, doi:10.1002/2015JA021166.

Sagdeev, R. Z. (1966), Cooperative phenomena and shock waves in collisionless plasma, in *Reviews of Plasma Physics*, vol. 4, edited by M. A. Leontovich, p. 23, Consultants Bureau, New York.

Sergeev, V. A., R. J. Pellinen, and T. I. Pulkkinen (1996), Steady magnetospheric convection: A review of recent results, *Space Sci. Rev.*, *75*, 551–604, doi:10.1007/BF00833344.

Sorathia, K. A., V. G. Merkin, A. Y. Ukhorskiy, B. H. Mauk, and D. G. Sibeck (2017), Energetic particle loss through the magnetopause: A combined global MHD and test-particle study, *J. Geophys. Res.*, *122*, 9329, doi:10.1002/2017JA024268.

Terasawa, T. (1979), Energy spectrum and pitch angle distribution of particles reflected by MHD shock waves of fast mode, *Planet. Space Sci.*, *27*, 193.

Thorne, R. M. (2010), Radiation belt dynamics: The importance of wave - particle interactions, *Geophys. Res. Lett.*, *37*, L22,107, doi:10.1029/2010GL044990.

Turner, D. L., V. Angelopoulos, S. K. Morley, M. G. Henderson, G. D. Reeves, W. Li, D. N. Baker, C.-L. Huang, A. B. H. E. Spence, S. G. Claudepierre, J. B. Blake, and J. V. Rodriguez (2014), On the cause and extent of outer radiation belt losses during the 30 september 2012 dropout event, *J. Geophys. Res.*, *119*, 1530, doi: 10.1002/2013JA019446.

Ukhorskiy, A. Y., M. I. Sitnov, V. G. Merkin, and A. V. Artemyev (2013), Rapid acceleration of protons upstream of earthward propagating dipolarization fronts, *J. Geophys. Res.*, *118*, doi:10.1002/jgra.50452.

Ukhorskiy, A. Y., M. I. Sitnov, R. M. Millan, B. T. Kress, J. F. Fennell, S. G. Claudepierre, and R. J. Barnes (2015), Global storm time depletion of the outer electron belt, *J. Geophys. Res.*, *120*, doi:10.1002/2014JA020645.

Ukhorskiy, A. Y., M. I. Sitnov, V. G. Merkin, M. Gkioulidou, and D. G. Mitchel (2017), Ion acceleration at dipolarization fronts in the inner magnetosphere, *J. Geophys. Res.*, *122*, doi:10.1002/2016JA023304.

Vasyliunas, V. (1984), Fundamentals of current description, in *Magnetospheric Currents*, *Geophys. Monogr. Ser*, vol. 28, edited by T. A. Potemra, p. 63, AGU, Washington, DC.

Williams, D. J. (1987), Ring current and radiation belts, *Reviews of Geophysics*, *25*, 570, doi:10.1029/RG025i003p00570.

Wiltberger, M., V. Merkin, J. G. Lyon, and S. Ohtani (2015), High-resolution global magnetohydrodynamic simulation of bursty bulk flows, *J. Geophys. Res.*, *120*, 4555, doi: 10.1002/2015JA021080.

Zhou, X.-Z., V. Angelopoulos, V. A. Sergeev, and A. Runov (2010), Accelerated ions ahead of earthward propagating dipolarization fronts, *J. Geophys. Res.*, *115*, A00I03, doi:doi:10.1029/2010JA015481.

Zhou, X.-Z., V. Angelopoulos, V. A. Sergeev, and A. Runov (2011), On the nature of precursor flows upstream of advancing dipolarization fronts, *J. Geophys. Res.*, *116*, A03,222, doi:doi:10.1029/2010JA016165.